



Numerical Visualization of Plunging Water Jet using Volume of Fluid Model

A. Boualouache^{1†}, F. Zidouni² and A. Mataoui²

¹ Department of Mechanical Engineering, Faculty of Technology, University of A. Mira Bejaia, 06000, Bejaia, Algeria.

² Laboratory of Theoretical and Applied Fluid Mechanics, Faculty of Physics, University of Science and Technology Houari Boumediene - USTHB, Algiers, Algeria.

†Corresponding Author Email: amine.boualouache@univ-bejaia.dz

(Received April 12, 2017; accepted October 5, 2017)

ABSTRACT

A plunging liquid jet is defined as a moving column of liquid passing through a gaseous headspace, air in our case, before impinging a free surface of receiving liquid pool. The mechanism of air entrainment due to plunging liquid jets is very complex and the complete mechanism of air entrainment is not fully understood so far. The present paper is an unsteady numerical simulation of air entrainment by water jet plunging, using the Volume Of Fluid (VOF) model. The piece wise linear interface construction algorithm (PLIC) for interface tracking is used, to describe the phase distributions of entirely immiscible air and liquid phases. The aim of this work is to investigate the performance and accuracy of the VOF method in predicting the initial impact between the descending jet and water free surface, air entrainment and the developing flow region under free surface. Three scale models based on geometric similarities (Froude number and dimensionless free jet length) are used for validation according to [Chanson \(2004\)](#) experience. The simulations show with accuracy, the air cavity formation steps, caused by the initial jet impact, its deep stretching under the pool free surface, until breakdown due to the shear created by a toroidal vortex. In terms of, air entrainment estimation, bubble dispersion and radial distribution of air volume fraction, large-scale models present a good agreement with the experience. However, for the smallest scale model, the results lead to suggest that air entrainment is governed by more parameters than the geometric similarities.

Keywords: Air entrainment; CFD; Two phase flow; Volume of fluid; Air cavity; Water plunging jet.

NOMENCLATURE

D	tank diameter	U_0	Initial velocity
$D^\#$	dimensionless turbulent diffusivity	$x_{\alpha max}$	distance normal to the center line where $\alpha = \alpha_{max}$
d	jet diameter	z	axial coordinate
d_i	jet diameter at the impinging point	σ	interfacial tension
Fr	froude Number $Fr=U_z/\sqrt{gd}$	μ	viscosity
g	acceleration due to gravity	ρ	density
h	free jet length	α	volume Fraction
I_0	bessel function		
k	surface curvature		
l	turbulent length scale		
p	fluid pressure		
Q	masse flow rate		
u	axial mean velocity		
U	velocity components		

subscripts

air air flow
w water flow

1. INTRODUCTION

Plunging jet entrainment is a highly efficient mechanism for producing large gas-liquid interfacial areas. In chemical engineering, plunging jets are used to stir chemical as well as to increase gas-liquid

transfer ([McKeogh and Ervine, 1981](#), [Bin, 1993](#)). In sewage and water treatment plants, aeration cascades combine the effects of flow aeration and high turbulence level, enhancing the mass transfer of volatile gases (Oxygen, nitrogen, volatile organic compounds). In the oceans, plunging breaking waves

can entrain a large amount of air bubbles when the top of the wave forms a water jet projecting ahead and impacts the water free surface in front of the wave, [Griffin \(1985\)](#).

Generally, air entrainment could be seen as a consequence of two complementary mechanisms: the first one, the interfacial shear along the liquid jet interface, which drags down an air boundary layer. The second one is the air entrapment process at the impinging point of the plunging jet with the receiving pool. This entrapment forms a transient relatively large air cavity with its cylindrical bottom part pinching off, thus generating air bubbles, [Zhu \(2000\)](#). Afterwards, the air bubbles go deeper and form an air plume below the water level.

In the seventies, there were only a few attempts to study the phenomenon of air entrainment by plunging liquid jets. Since then, the interest on plunging jet systems have increased considerably, [Bin and Smith \(1982\)](#); [Bin \(1988c\)](#). So far, several investigations have been carried out to understand the mechanisms related to the air entrainment by plunging jet, [Roya \(2013\)](#), [Harby \(2014\)](#), and most of the achieved results are based on empirical and semi-empirical models.

Several researchers, [Bonetto and Lahey \(1993\)](#); [Cummings and Chanson \(1997\)](#); [Lucas \(2008\)](#), highlighted the lack of information on the air comportment near the impinging point and on the entrained bubble size distributions. Therefore, a consistent approach able to take into account all the parameters that govern the entrainment phenomenon and the stability of the jet (free surface instabilities, the turbulence, velocity profile) is still missing. Furthermore, physical models of plunging jet flows remain a subject of some scaling effects tried to be explained by [Wood \(1991\)](#), [Chanson \(2004\)](#), and [Zidouni \(2011\)](#). They noticed that the generation of bubbles happens on a scale which is smaller than the bubbles, this process cannot be resolved in meso-scale simulations, which include the full length of the jet and its environment.

With the increase of the available computers power in the last decade, several numerical models have been developed to contribute for the best understanding of multiphase flows including plunging jet.

Volume of Fluid, which is introduced by [Hirt and Nichols \(1981\)](#), is one model of choice to reproduce the interface motion in the simulation of multi-fluids flows.

It was implemented in numerous works for tracking the free surface motion, [Mirzaii \(2012\)](#), the deformation of the liquid-gas interface in containers [Elahi \(2015\)](#) and liquid sloshing in tanks with internal baffles, [Alireza \(2013\)](#). It was integrated in hybrid multifluid-VOF model to enable simulation of both the initial jet impingement and the long-time entrained bubble plume phenomena, [Olabanji \(2015\)](#).

In plunging jet configurations, many works in the literature employed VOF model. [Qu \(2011\)](#) analyzed

using VOF model, the process of air carry under by liquid plunging jet. The air cavity caused by the jet impact deeply stretches under the pool surface until breakdown due to the shear created by vortex. The predicted maximum height of the developing air cavity, the velocity of the front of the air cavity show very good agreement with existing semi-empirical correlations from the literature and experiments.

[Suraj \(2013\)](#) employed VOF methodology to study the air entrainment characteristics of a water jet plunging into a quiescent water pool at angles ranging from $\theta = 10^\circ$ to $\theta = 90^\circ$ measured from the horizontal. Their results shows that the entrained air volume increases considerably from normal impingement to shallow angles and the size of cavities formed around the jet likewise increases at shallower angles.

[Khezzar \(2015\)](#) used large eddy simulation based on the Smagorinsky dynamic sub-grid scale model in combination with the multiphase VOF model, to simulate the flow of two turbulent plunging water jets. A weakly disturbed jet with low turbulence content and a highly disturbed jet with a profile almost fully developed at the exit. The simulation captured successfully the previous experimentally observed topological phenomena taking place during the transient impact and continuous entrainment regime. It showed that surface instabilities in the free jet, due to its turbulence content have remarkable effect on submerged interfacial area, air volume, and air-entrainment rate.

The present paper is devoted to study air entrainment by water plunging jet using VOF Multiphase model. The governing equations, in three-dimensional coordinates system, are solved using the commercial CFD code ANSYS-Fluent. The interface between the two fluids is reconstructed by the implementation PLIC algorithm in 3D version according to CSF model, of [Brackbill \(1992\)](#). It is used successfully for large velocity hydrodynamic calculations by a host of researchers, [Rider \(1995\)](#), [Puckette \(1997\)](#).

The objective of this study is therefore the numerical investigation of applicability and accuracy of VOF model to reproduce a transient circular liquid plunging jet on a quiescent pool and the air plume formed underneath it. The analyze focused on the jet surface behavior beneath the impact region, mainly the air cavity formation, the air plume development and progression and the velocity field around that region. Particular attention is given to air volume fraction distribution in different layers of the plume and its corresponding air entrainment rate.

The results are compared and validated against semi-empirical correlations from the literature and experimental evidence, [Chanson \(2004\)](#).

The numerical model provides an overview on the mechanism of air entrainment by a liquid plunging jet and reports some topological features during and after the transient impact of a free turbulent plunging jet

2. Mathematical Modeling

VOF model, [Hirt and Nichols \(1981\)](#), is based on the

one-fluid multiphase concept. The formulation uses a single set of conservation equations. Hence only one velocity field is computed. The material properties of the mixture are calculated by a volume fraction average of all fluids in the cell. The volume fraction of each fluid in the computational cells is tracked throughout the entire computational domain. In addition to the velocity and pressure, the volume fraction depends on the flow field; it appears in both mass and momentum equations. These variables are shared by the two phases and correspond to volume-averaged values as described in Eqs. 3, 5 and 6.

VOF model shows more flexibility and efficiency than other models for tracking liquid–gas interfaces, so that it has been widely used in analyzing various two-phase flow systems, where the change of interface is important such as in coalescence and break-up, [Lakehal \(2002\)](#), [Rider \(1998\)](#).

Time evolution of the interface between these two immiscible fluids is followed in the computational domain using PLIC model to track sharp interfaces without large numerical diffusion. It assumes that the interface between the two fluids has a linear shape within each mixed cell and uses this linear shape to calculate the advection of fluid through the cell faces.

Following [Youngs \(1982\)](#), the first step in their construction scheme is calculating the position of the linear interface relative to the center of each partially filled cell, using information about volume fraction and its derivatives in the cell. The second step is calculating the advecting amount of fluid through each face using the computed linear interface representation and information about the normal and tangential velocity distributions on the face. Finally, the volume fraction in each cell is obtained using the balance of fluxes calculated during the previous step.

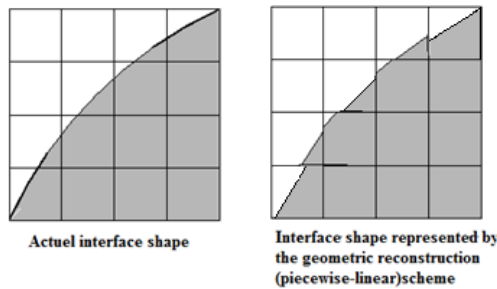


Fig. 1. Interface reconstruction using PLIC method, [Rider \(1995\)](#).

In this work, the flow field is considered incompressible and statistically unsteady. The momentum equation for computational domain in its generalized form is written as:

$$\nabla \cdot U = 0 \quad (1)$$

$$\frac{\partial \rho U}{\partial t} + \nabla \cdot \rho U = -\nabla p + \nabla \cdot (\mu \nabla U) + \rho g + F_{sv} \quad (2)$$

Where, g and p are the gravity acceleration and pressure, respectively. The volume fraction α of the primary phase, (water in our case) has the following

form:

$$\frac{\partial \alpha}{\partial t} + U \cdot \nabla \alpha = 0 \quad (3)$$

Whereas α_{air} is air volume fraction defined:

$$\alpha_{air} = 1 - \alpha \quad (4)$$

In each control volume, the volume fraction of all phases sum to unity. The proprieties appearing in the transport equation namely density ρ and the viscosity μ of the mixture are defined by a linear weighing of both water and air density and viscosity respectively, are deduced from Eqs. 5 and 6:

$$\rho = \rho_{air}(1 - \alpha) + \rho_w \alpha \quad (5)$$

$$\mu = \mu_{air}(1 - \alpha) + \mu_w \alpha \quad (6)$$

In the developed method of [Brackbill \(1992\)](#), the continuum surface force (CSF) method replaces the requiring to define the exact location of the free surface by converting the surface tension into an equivalent volume force. It is coupled to momentum equations as an additional body force. This force has smoothed properties and acts only in a finite transition region across the interface, which contains the interfacial and their immediate neighboring cells. It is determined by the following expression:

$$F_{sv} = \sigma \frac{\rho_w}{\frac{1}{2}(\rho_{air} + \rho_w)} k \nabla \alpha \quad (7)$$

Where σ is the free surface tension. $\nabla \alpha$ and k are defined as the water volume fraction gradient and the air–water interface curvature respectively.

$$k = -\nabla n \quad \text{and} \quad n = \frac{\nabla \alpha}{\|\nabla \alpha\|} \quad (8)$$

Although it is known that turbulence near interfaces separating two immiscible fluids can be strongly anisotropic involving rapid and complex deformations, breaking, and merging. In this study, for the sake of simplicity and practical computing time, the standard k – ϵ turbulence model is adopted, [lauder \(1974\)](#).

3. Numerical Procedure

The flow is simulated basing on the mathematical model VOF implemented in the CFD code ANSYS-Fluent. Pressure based solver is used considering explicit volume fraction and implicit body force formulation. Three scale models based on geometric similarities (Froude number and dimensionless free jet length) are used for validation according to [Chanson experience \(2004\)](#), see Table (2).

The geometry grid and boundary conditions are shown in Fig. 2, where a quadrilateral non-uniform mesh is used. A clustering is required toward the water jet centerline and the water free surface in order to track the air and water flows, also the deformation of the air-liquid interface. The smallest bubble size observed in the plunging jet experiment is about 1mm; hence, the cell sizes are maintained to

be the same size of the smallest bubbles in the whole plume region. However, the large cells are located outside perimeter of the plume region. At the centerline, the cells are quadratic and have a good quality in term of skewness factor and orthogonal quality, [Mahaffy \(2007\)](#).

Table 1 Grid sensitivity of the three scale models using air entrainment ratio

geometry	Grid size (nodes)		Air entrainment
Scale model-1	coarse	87500	0.320
	medium	437500	0.220
	fine	980000	0.210
Scale model-2	coarse	71991	0.250
	medium	147000	0.188
	fine	208000	0.170
Scale model-3	coarse	68546	0.290
	medium	130680	0.202
	fine	190540	0.185

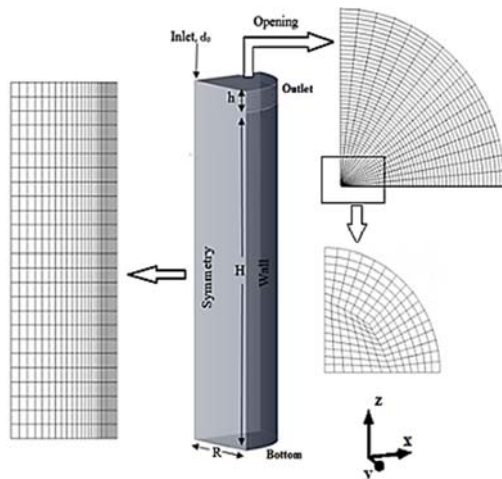


Fig. 2. Computational grid arrangement and boundary conditions.

Grid convergence tests were achieved for the three different scale models. Three different grids were used coarse, medium and fine. The comparison was performed using the air entrainment ratio. The results are summarized in Table (1), where the results from the medium and fine meshes are close to each other. Hence, the medium size grid of was adopted for all the cases studied.

At the nozzle inlet, uniform velocity profile is considered. At the walls, no slip conditions for the fluids were applied. The upper section of the domain is modeled as an opening boundary condition with a relative pressure of 0 Pa, where as the outflow is set at the lateral section of the tank assuming pressure outlet boundary condition. As the computational domain is reduced, a symmetry boundary condition is consequently used at symmetry planes. The initial flow conditions are set for the water level.

Mass flow rates of outlet boundaries are less 10^{-6}

providing an acceptable mass balance. The spatial derivatives in the conservation equations were discretized using quick scheme while Geo-Reconstruct was applied in the discretization of the volume fraction in Eq. (3). The PISO algorithm was used for pressure-velocity coupling. Time discretization used a first order implicit scheme for the conservation equations.

3.1. Modeling Parameter

Figure (2) shows a geometry of the computational domain referring to three cases carried out by [Chanson \(2004\)](#). These three-scale models are of different jet and vessel dimensions as detailed in Table (2). However, similar boundary conditions are considered.

4. RESULTS AND DISCUSSION

The process of initial impact and development of the air cavity leading to continuous entrainment is discussed. The spatial and temporal variations of the cavity depth until the pinch-off are discussed and contrasted with results of empirical correlations taken from the literature.

For the air plume development, the vertical air flux, the entrainment rate and the radial distribution of the air volume fraction in different layers below water free surface are discussed and compared to the experimental results and empirical correlations available in literature.

In a first step, the calculation performed with the full geometry domain for scale model- M1 nevertheless, in sake of decrease calculations time, the quarter of the geometry is adopted, where a good agreement is obtained with the two configurations, see Fig. 3.

4.1. Initial Impact and Air Cavity Development

Figure (3) shows chronological changes of the impact region between the descendent jet and the pool water free surface. It is about series of instantaneous phase concentration distributions for the case of Scale Model-1(see Table (2)), obtained from the numerical simulations.

When the jet strikes the free liquid surface around 0.08s, a shallow depression at the impact point is created and filled by air. Gradually, it reaches a cylindrical form around $t=0.12s$, which we call an air cavity.

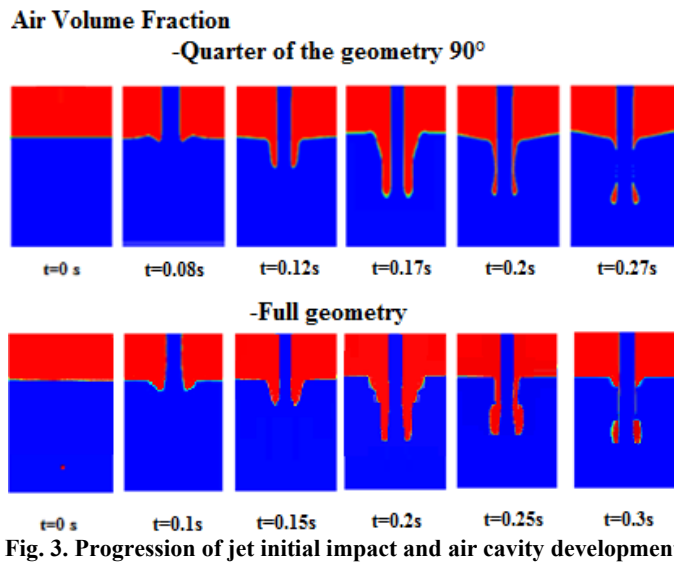
The air cavity stretches in length and becomes thinner, around $t=0.2s$. That decrease its resistance to the surrounding liquid, Fig. 4. Around $t=0.27s$ it pinches off and collapses along its vertical axis. The cavity narrowed in size and the top part of the broken cavity tries to entrain the free liquid surface upward toward its initial position around the jet.

4.2. Air Cavity Dimensions

The initial air cavity dimensions provides a quantitative evaluation of VOF model ability to capture the air cavity details. Semi-analytical relations have been developed by [Zhu \(2000\)](#) to

Table 2 Modeling parameters for different simulated scale models

	parameters	CHANSON experiment		
		Scale Model-M1	Scale Model-M2	Scale Model-M3
Flow Properties	Water density (kg/m ³)	997	997	997
	Water dynamic viscosity(Pa s)	1.01 10 ⁻³	1.2210 ⁻³	1.22 10 ⁻³
	Surface tension (N/m)	0.055	0.073	0.073
Geometry of Test Section	Vessel diameters D=2.R (m)	0.3	0.1	0.1
	Vessel height H (m)	1.8	0.75	0.75
	Nozzle diameter d (m)	0.025	0.0125	0.00683
	Free jet length h (m)	0.1	0.05	0.0273
	Dimensionless jet length (h/d)	4.0	4.0	4.0
Flow Conditions	Inlet Velocity(m/s)	4.1	3.04	2.16
	Froude Number	8.5	8.5	8.5



estimate diameter and the initial penetration depth of the air cavity below the undisturbed pool surface before it collapse.

$$\frac{l}{d_j} = \frac{1}{4} \left(\frac{D_c}{d_j} \right)^{2/3} Fr^{1/3} + 2cFr^{1/4} \quad (9)$$

$$\frac{D_c}{d_j} = 2cFr^{1/4} \quad (10)$$

$$\frac{D_h}{d_j} = 2.41 \quad (11)$$

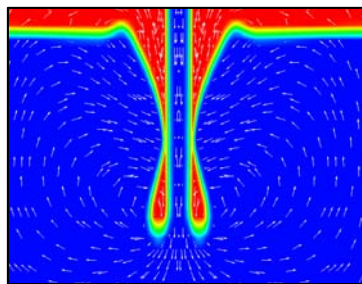


Fig. 4. Pinch-off of air cavity.

Where d_j is the jet impinging diameter, D_c the diameter of the approximated hemisphere formed at the impact, D_h the diameter of the cylindrical part of the cavity and c a constant value of 0.9.

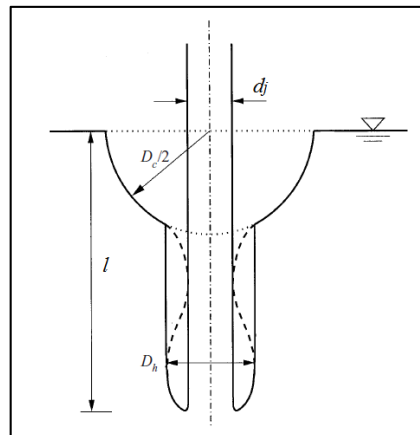


Fig. 5. Geometric dimensions of the underwater air cavity.

The semi-analytical values obtained from Eqs. (09), (10) and (11) of the air cavity geometrical dimensions are presented in Table (3) with those resulting from the numerical simulations for the three different configurations.

Table 3 Air cavity dimensions of the three different scale models

		Scale Model-1	Scale Model-2	Scale Model-3
D_c (cm)	Eq-10	7.70	3.80	2.10
	CFD	8.0	3.50	2.30
D_h (cm)	Eq-11	6.02	3.01	1.64
	CFD	4.54	2.25	1.40
$\frac{D_h}{d_j}$	Eq-11	2.41	2.41	2.41
	CFD	1.81	1.80	2.04
$\frac{D_c}{d_j}$	Eq-10	3.08	3.04	3.07
	CFD	3.2	2.8	3.36
l (cm)	Eq-09	10.38	5.18	2.83
	CFD	6.713	4.5	2.54

The estimated constant value of D_h/d_j from Eq. (11) is 2.41, whereas the estimated values obtained from the numerical simulations are relatively smaller than 2.41 with a maximum error of 25%.

Looking at D_c/d_j in Table (03), Eq. (10) is in good agreement with the numerical predictions with an error ranging to 8%.

For the air cavity depth, the estimated values from the numerical simulation are smaller than the empirical values of Eq. (09). The maximum error between numerical simulations and Eq. (09) for the third scale model, and reaches up to 25 %.

It has noticed that the values reported in Table (3) show coherent evolution of air cavity depth according to the geometry scale. The air cavity depth of any arbitrary scale can be deduced from the air cavity depth of a given scale that can be taken as reference scale, considering the same Froude Number. Hence, it can be correlated giving to Eq. (12). The results is given with error less than 15%:

$$l_s = \frac{C_0 l_1}{2^n} \quad (12)$$

l_s is the cavity depth of the small scale.

l_1 is the cavity depth of the large scale.

C_0 is a constant $C_0 = 1.2$.

n is the scale factor.

4.3. Air Plume development

After four seconds of physical time, Fig. 6 shows the air plume generated under the water free surface for Scale Model-1, which reaches a quasi-steady form. The air entrainment happens when the descendent flow jet carries under a quite air around the water jet column, referring to Eq.02 and the graph presented in Fig. 7. Hence, the velocity vectors reveal the presence of the toroidal liquid vortex (see close-up in Fig. 4). This vortex motion is responsible for the

subsequent pinch-off of the air cavity, as described above. Similar observation are notices by [Lahey \(2009\)](#) and [Qu \(2011\)](#).

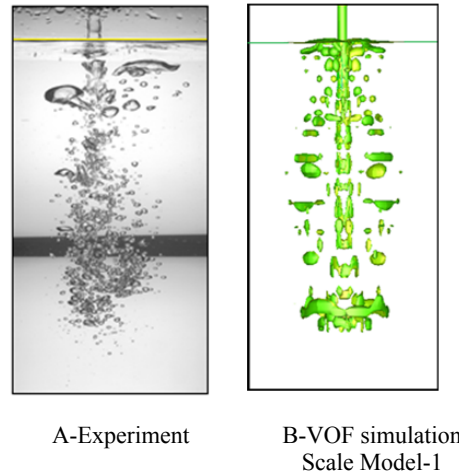


Fig. 6. Air entrainment illustration.

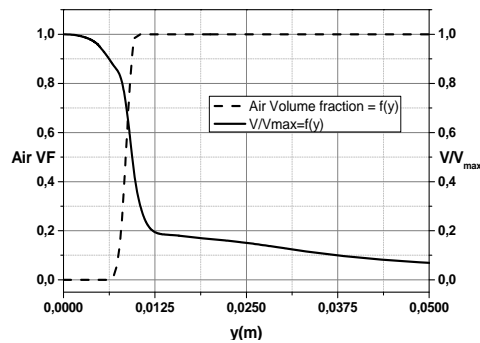


Fig. 7. Radial distribution of air volume fraction and velocity profile above the impact region.

The Fig. (8) illustrates flow sequences, from the pinching-off of air cavity until the full air plume generation, pictured at different times. After the pinch off, the bottom part of the broken cavity form a large toroidal, which surrounds part of the broken liquid jet, detaches from the bottom of the structure and collapses into a single large air bubble from, $t=0.2s$. It then disintegrates continuously into small bubbles. Thus, the bubbles formed are advected by the downward flow, then rise again by the effect of the buoyancy and form the air plume, $t=4s$; as presented in Fig.6-B and Fig. 8. This process is similar with the one described by, [Zhu \(2000\)](#), [Galimov \(2010\)](#) and [Qu \(2011\)](#).

While rising, large bubbles are numerically formed by coalescence. This behavior occurs when the mutual distances between two bubbles is less than the size of the computational cell, [Annaland \(2005\)](#). Therefore, the bubble size distribution could not be compared to the measured distribution. However, the overall developed plume is qualitatively similar to the experimental observations.

For the top part of the broken cavity, the process may repeat itself but the cavities created are of much

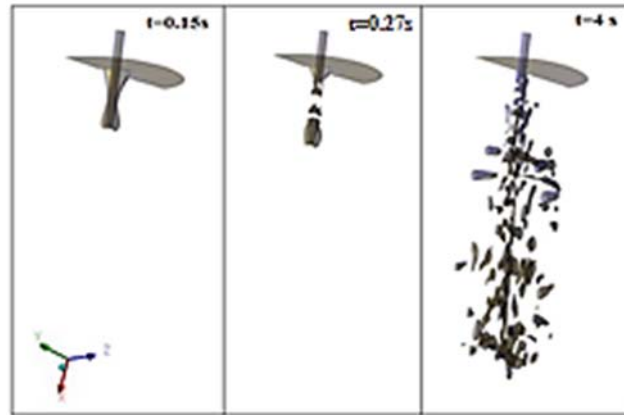


Fig. 8. A front view of air plume progression for scale Model-1.

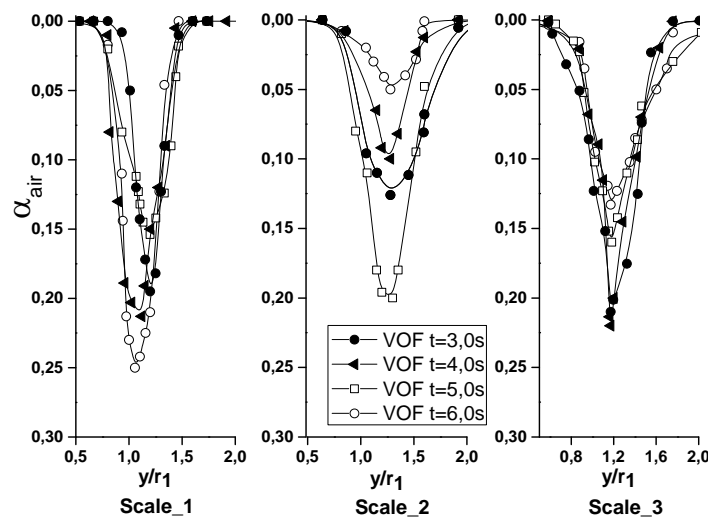


Fig. 9. Radial distribution of air volume fraction for the three different configurations at different time steps.

smaller sizes than the initial one because of the continuous interactions between the free liquid surface and the penetrating jet at the impact. This is appear clearly in Fig. 8 at $t=0.15s, 0.27s$ and $4s$.

4.4. Time Evolution of Air Volume Fraction Distribution

Figure (9) shows that the three scale models exhibit an air entrainment. The radial distribution of the air volume fraction has a pulsatile character and the simulation results are time dependent. The comparison with the experience is done within the averaged values over time from the steady state to the end of the simulation. The steady state is reached after 4 seconds simulation when the plume attains its full size.

The bubbles have discrete distribution within the plume and are not azimuthally symmetric. Consequently, an average over space is needed to smooth the air volume fraction distribution over a small section, corresponding to the radial location of the measurement. The averaging in space is done by space monitoring in the present CFD code Fluent.

The double average over time and space is performed according to the following equation:

$$\alpha = \frac{\iint_{s,t} \alpha(r,t) ds dt}{\iint_{s,t} ds dt} \quad (13)$$

Where ds is the annular section at radial position r within the width of 01 mm.

4.5. Air Entrainment Rate

Air entrainment ratio is calculated for the three different scale models, the results are presented in Table (4). It is defined considering the ratio of the vertical downward air flux over the inlet water jet flux. In general, the vertical air flux is estimated according to Eq.(17) considering only the downward air flux. In fact, the product of the air volume fraction α_{air} and vertical air velocity U_z defines the vertical air flux density q_{air}

$$q_{air} = \alpha_{air} \cdot U_z \quad (14)$$

Table 4 Results summary for air entrainment ratio in the three test cases

		Correlations		Chanson Experiment	VOF Model
		Van de Donk	Bin		
Q_{air}/Q_w	Scale Model1	0.221	0.126	0.178	0.220
	Scale Model2	0.221	0.126	0.240	0.188
	Scale Model3	0.221	0.126	0.070	0.202

To avoid considering both downward and upward air flux, a separate calculations of the two

Fluxes are distinguished by the following equations:

$$q_{air}^- = \begin{cases} q_{air} & \text{if } q_{air} < 0, \\ 0 & \text{else} \end{cases} \quad (15)$$

$$q_{air}^+ = \begin{cases} q_{air} & \text{if } q_{air} > 0, \\ 0 & \text{else} \end{cases} \quad (16)$$

Hence, the total downward air flux at a given level below the surface is given by:

$$Q_{air}^-(z = z_i) = \int_{z=z_i} q_{air}^- dS \quad (17)$$

Where S is the horizontal cross-section of the domain at a given level below the surface. z_i is the cross-section location under water free surface.

The total upward fluxes calculated with the same way.

A comparison of the air entrainment rate to those obtained by Bin (1993) and Van de Donk (1981) correlations is performed. These both correlations are based on the dimensionless scale models, that Chanson has chosen as similitude parameter namely (Fr and h/d). Hence, the air entrainment rate remains unchanged.

Good agreement to Van de Donk (1981) correlation is obtained for the three scale models. Nevertheless, experimental discrepancies highlight the sensitivity of the small scalemodel-M3 to more parameters than those considered (Froude number and dimensionless free jet length).

Van de Donk (1981)

$$Q_{air} / Q_w = 0.09(h/d)^{0.65} \quad (18)$$

Bin (1993)

$$Q_{air} / Q_w = 0.04 Fr^{0.28} (h/d)^{0.4} \quad (19)$$

4.6. Radial Distribution of Air Volume Fraction

Similar air volume fraction distribution profiles to the experimental ones are obtained for the three scale models. Quantitatively, the first scale model which is the largest one ($d_j=2,5\text{cm}$) shows a better

agreement to the experimental measurement of the maximum air volume fraction by 15% of precision. Similarly to the Chanson correlation for smaller scale model M3 ($d_j=0,68\text{cm}$), the discrepancy is larger. An expansion of the plume due to air diffusion layer is visibly occurred in scale model M3. However, the overall results are in good agreement in comparison to Chanson correlation defined by Eq. (20) and plotted in Fig.10.

$$\alpha = \frac{Q_{air}}{Q_w} \frac{1}{4D^\# (z-h)/x_{cmax}} \times \exp\left(\frac{1}{4D^\#} \frac{(r/x_{cmax})^2}{(z-h)/x_{cmax}}\right) \cdot I_0\left(\frac{1}{2D^\#} \frac{r/x_{cmax}}{(z-h)/x_{cmax}}\right) \quad (20)$$

Where $D^\#$ is the dimensionless turbulent diffusivity, x_{cmax} , the perpendicular distance to the centerline, matching with $\alpha=\alpha_{max}$ and I_0 is the modified Bessel function of the first kind of order zero.

In each scale model, the attenuation of the air plume depends on the diminution of the maximum air volume fraction in each cross section. However, in the numerical prediction the plume attenuation is somewhat appeared. Due to the mathematical modeling that considers a null slip velocity between the two phases, (see Eq .2).

5. CONCLUSION

Numerical simulation of circular water jet plunging into a quiet pool is carried out using VOF model where, the interface reconstruction between the two phases is performed according to PLIC algorithm. Validation is performed according to Chanson experiments (2004). For similitude consideration, three jet sizes representing three different scale models were considered. Hence the corresponding data implies same inflow conditions namely Froude number and dimensionless jet length ($h/d=4.0$, $Fr=8.5$).

VOF model proves its performance to reproduce the initial impact of the descending jet with the water free surface, surface deformation, dimensions and progression of the air cavity until pinch-off for three different scale models.

Initially, a semi-spherical air cavity is created, changes in shape to attain a conical section followed later by a cylindrical section. The cavity collapses in the cylindrical part, due to the induced vortex motion. A large toroidal air bubble detaching and moving downwards.

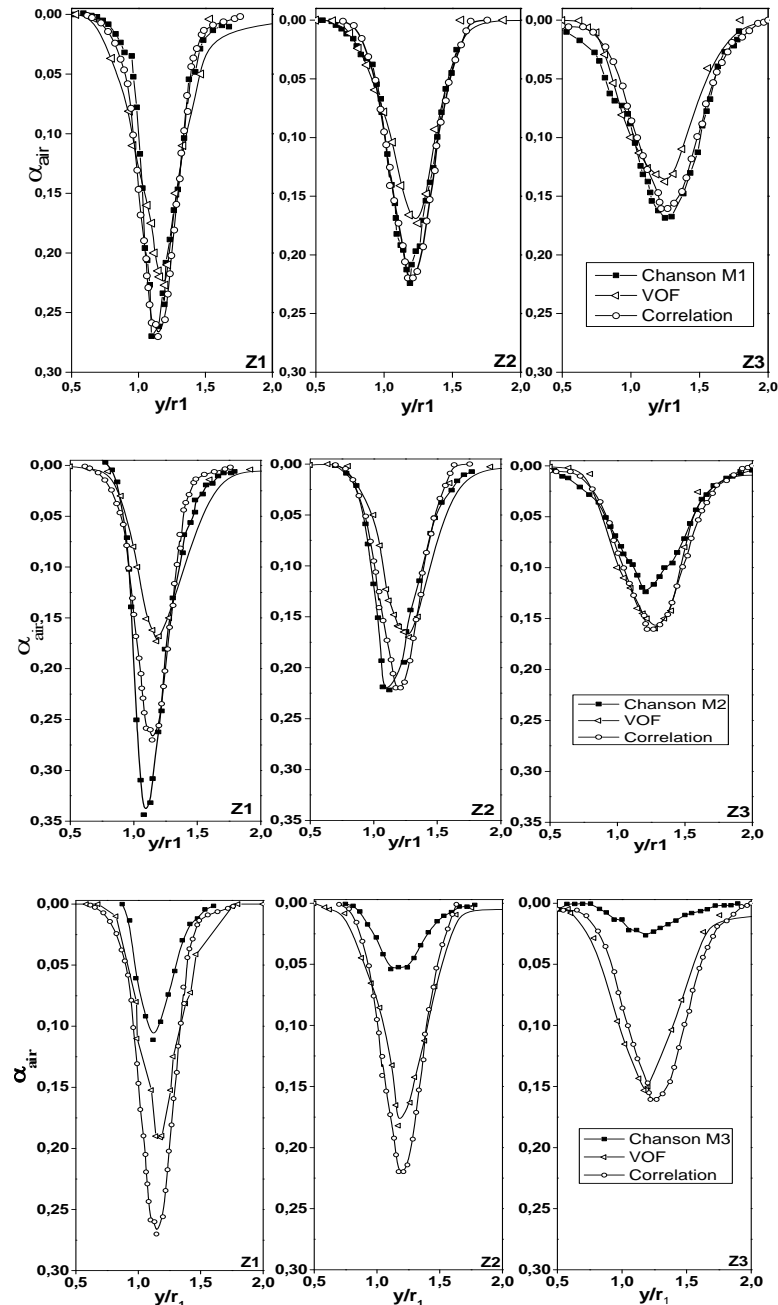


Fig. 10. Air volume fraction distribution (α_{air}) for identical inflow conditions ($h/d=0.4$, $Fr=8.5$)- Comparison between VOF method and Chanson experience (2004), $(z-h)/d_1=1.6$; $(z-h)/d_1=2.5$; $(z-h)/d_1=4.1$.

It is noticed that air cavity depth has coherent evolution according to the geometry scale, from any arbitrary scale; Eq. (12), the air cavity depth of can be deduced from the air cavity depth of a given scale that can be taken as reference scale, considering the same Froude Number.

Focusing on the developing region, the radial distribution of air volume fraction shows a maximum air volume fraction at the periphery of the jet ($r \approx r_{jet}$). In the experiment, this maximum decays exponentially for deeper locations. However, in the numerical simulation it remains almost constant since the two phases are moving with the same velocity. This fact

is inherent to the VOF modeling which resolve only one equation. Hence, no slip velocity between the two phases could be modeled.

Good agreement of air entrainment rate is noticed for the two large scale-models M1 and M2 but overestimated in case the smallest scale model M3. Chanson (2004) has noticed same tendency using correlation based on Froude number and dimensionless free jet length. This result leads to suggest that the entrainment is governed by more parameters than the geometric similarities. Hence, small scale-models should be more investigated to define the whole mechanism of the air entrainment.

REFERENCES

- Alireza, J., R. Elahi and M. Passandideh Fard (2013). Numerical Simulation of liquid Sloshing with baffles in the fuel container. *The 12th Iranian Aerospace Society Conference*. Amir Kabir University of Technology. AERO2013-17469.
- Annaland, M. S., Deen, N. G., Kuipers, J. A. M. (2005). Numerical simulation of gas bubbles behavior using a three-dimensional volume of fluid method. *Chem. Eng. Sci.* 60 2999–3011.
- Bin, A. K. (1993). Gas entrainment by plunging liquid jets. *Chem. Eng. Sci.* 48(21), 3585-3630,
- Bin, A. K. and Smith (1982). Mass transfer in a plunging liquid jet absorber. *Chen Engng commun.* 15.367-383.
- Bin, A. K. (1988c). Gas entrainment by plunging liquid jets. *VDI for schungsh.* 648/88,1-36.
- Bonetto, F. and R. T. Lahey (1993). An experimental study on air carry-under due to a plunging liquid jet. *Int. J. Multiphase Flow* 19, 281 – 294.
- Brackbill, J. U., D. B. Kothe and C. Zemach (1992). A continuum method for modeling surface tension. *J. Comput. Phys.* 100, 335–354.
- Chanson, H., S. Aoki and A. Hoque (2004). Physical modeling and similitude of air bubble entrainment at vertical circular plunging jets. *Chemical Engineering Science.* 59 747 – 758,
- Cummings, P. D. and H. Chanson (1997a). Air entrainment in the developing flow region of plunging jets. *J. Fluids Eng.* 119, 597–602,
- Elahi, R., M. Passandideh Fard and A. Javanshir (2015). Simulation of liquids sloshing in 2D containers using the volume of fluid method. *Ocean Engineering* 96, 226–244.
- Galimov, A. Y., O. Sahni, R. T. Lahey, M. S. Shephard D. A. Drew and K. E. Jansen (2010). Parallel adaptive simulation of a plunging liquid jet. *Acta Math. Sci.* 30B (2), 522–538.
- Griffin, O. M. (1985). Vortex shedding From Bluff Bodies in a Shear Flow. *J. Fluids Eng* 107(3), 298-306.
- Harby, K. and al. (2014). An experimental study on bubble entrainment and flow characteristics of vertical plunging water jets. *Journal of Experimental Thermal and Fluid Science.* 57 207–220.
- Hirt, C. W. and B. D. Nichols (1981). Volume of fluid method (VOF) for the dynamics of free boundaries. *J. Comput. Phys.* 39, 201–225.
- Khezzar, L., N. Kharoua and K. T. Kiger (2015). Large eddy simulation of rough and smooth liquid plunging jet processes. *Journal of Progress in Nuclear Energy.* 85.140-155.
- Lahey, R. T. (2009). On the direct numerical simulation of two-phase flow. *Nucl. Eng. Des.* 239, 867–879.
- Lakehal, D., M. Meier and M. Fulgosi (2002). Interface tracking towards the direct simulation of heat and mass transfer in multiphase flows. *Int. J. Heat Fluid Flow* 23, 242–257.
- Lucas, D. (2008). Identification of relevant PTS scenarios, State of art of modeling and need model improvement, *European Commission 6th EURATOM Framework. Program 2005-2008 Integrated Project (IP): NURESIM Nuclear Reactor Simulations Sub-Project 2: Thermal Hydraulics,*
- Mahaffy, J. and *et al.* (2007). Best Practice Guidelines for the Use of CFD in Nuclear Reactor Safety Applications. *NES/CSNI/R* 5.
- McKeogh, E. J. and D. A. Ervine (1981). Air entrainment rate and diffusion pattern of plunging liquid jets. *Chem. Eng. Sci.* 36, 1191-1172.
- Mirzaii, I. and M. Passandideh Fard (2012). Modeling free surface flows in presence of an arbitrary moving object. *International Journal of Multiphase Flow.* 39, 216–226.
- Olabanji, Y. S. and E. W. Kent (2015). Numerical Investigation of Vertical Plunging Jet Using a Hybrid Multifluid–VOF Multiphase CFD Solver. *International Journal of Chemical Engineering*. Article ID 925639.
- Puckett, E. G. (1991). A volume of fluid interface tracking algorithm with applications to computing shock wave rare fraction. *In proceedings of the fourth international symposium on Computational Fluid Dynamics* 933-938.
- Qu, X., L. Khezzar and Z. Li (2011). The impact and air entrainment process of liquid plunging jets. *J. Process Mechanical Engineering.* 226.
- Rider, W. J. and D. B. Kothe (1995). Stretching and tearing interface tracking methods. *Presented at the AIAA CFD Conference, San Diego.* AIAA-95-1717.
- Rider, W. J. and D. B. Kothe (1998). Reconstructing volume tracking. *Journal of Computational Physics.* 141, 112–152.
- Roya, A. K. and all (2013). Visualization of air entrainment by a plunging jet. *Fifth BSME International Conference on Thermal Engineering-Procedia Engineering.* 56 468–473.
- Suraj, S. D. and F. T. Mario (2013). Distinguishing features of shallow angle plunging jets. *PHYSICS OF FLUIDS* 25, 082103.
- Vande Donk, J. (1981). Water aeration with plunging jets. *Ph.D. Thesis, TH Delft, the Netherlands* 168.
- Wood, I. R. (1991). Air entrainment in free-surface flows. *IAHR Hydraulic Structures Design Manual No. 4. Hydraulic Design Considerations, Balkema, Rotterdam, the Netherlands* 149.

A. Boualouache *et al.* / *JAFM*, Vol. 11, No.1, pp. 95-105, 2018.

Youngs, D. L., K. W. Morton and M. L. Baines (1982). Time-dependent multi-material flow with large fluid distortion. In *Numerical methods for fluid dynamics*. Academic Press, New York. (Eds K. W. Morton, M. J. Baines) 273–285.

Zhu, Y., H. N. Oguz and A. Prosperetti (2000). On

the mechanism of air entrainment by liquid jets at a free surface. *J. Fluid Mech* 404, 151–177.

Zidouni, K. F., E. Krepper, S. A. Bousbia, L. Dirk and A. Mataoui (2011) .Numerical study of a bubble plume generated by bubble entrainment from an impinging jet. *Nuclear Engineering and Design* 241 4111– 4121.